Journal of Environmental Management 316 (2022) 115329

Contents lists available at ScienceDirect

Journal of Environmental Management

journal homepage: www.elsevier.com/locate/jenvman

Research article

Role of Zr loading into In_2O_3 catalysts for the direct conversion of CO_2/CO mixtures into light olefins

A. Portillo, A. Ateka *, J. Ereña, J. Bilbao, A.T. Aguayo

Department of Chemical Engineering, University of the Basque Country, UPV/EHU, P.O. Box 644, 48080, Bilbao, Spain

ARTICLE INFO

Keywords:
CO_2 valorization
Syngas
In_2O_3–ZrO_2 catalyst
Olefins
Oxygenates
Catalyst deactivation

ABSTRACT

The effect of the ZrO_2 content on the performance (activity, selectivity, stability) of In_2O_3–ZrO_2 catalyst has been studied on the hydrogenation of CO_2/CO mixtures. This effect is a key feature for the viability of using In_2O_3–ZrO_2/SAPO-34 tandem catalysts for the direct conversion of CO_2 and syngas into olefins via oxygenates as intermediates. The interest of co-feeding syngas together with CO_2 resides in jointly valorizing syngas derived from biomass or wastes (via gasification) and supplying the required H_2. The experiments of methanol synthesis and direct synthesis of olefins, with In_2O_3–ZrO_2 and In_2O_3–ZrO_2/SAPO-34 catalysts, respectively, have been carried out under the appropriate conditions for the direct olefins synthesis (400 °C, 30 bar, H_2/CO_X ratio = 3) in an isothermal fixed bed reactor at low space time values (kinetic conditions) to evaluate the behavior and deactivation of the catalysts.

The Zr/In ratio of 1/2 favors the conversion of CO_2 and CO_X, attaining good oxygenates selectivity, and prevents the sintering attributable to the over-reduction of the In_2O_3 (more significant for syngas feeds). The improvement is more remarkable in the direct olefins synthesis, where the thermodynamic equilibrium of methanol formation is displaced, and methanation suppressed (in a greater extent for feeds with high CO content). With the In_2O_3–ZrO_2/SAPO-34 tandem catalysts, the conversion of CO_x almost 5 folds respect oxygenates synthesis with In_2O_3–ZrO_2 catalyst, meaning the yield of the target products boosts from ~0.5% of oxygenates to >3% of olefins (selectivity >70%) for mixtures of CO_2/CO_X of 0.5, where an optimum performance has been obtained.

1. Introduction

In the current transition period towards green energy, the implementation of carbon capture and utilization (CCU) strategies is one of the biggest challenges to achieve the goal of decarbonization and tackle climate change. In this scenario, the technological development of efficient routes for the large scale conversion of CO_2 into value-added products is imperative to offset the cost of its capture and storage (Hepburn et al., 2019; Kamkeng et al., 2021; Zhang et al., 2020).

The catalytic processes for the conversion of CO_2 into fuels and raw materials (as olefins and aromatics) receive great attention for their implementation in the refineries of the future (Garba et al., 2021; Leonzio, 2018; Ye et al., 2019) and are complemented by other initiatives aimed at intensifying the recovery of oil and natural gas (Alabdullah et al., 2020; Palos et al., 2021). As an alternative to the well-developed two-stage hydrocarbon production technologies from CO_2 hydrogenation to methanol/dimethyl ether (DME) (Sehested, 2019) and its selective conversion into olefins, gasoline or aromatics (Tian et al., 2015), hydrocarbon synthesis routes in one stage (modified Fischer Tropsch (MFT) or with oxygenates, methanol/DME, as intermediates), through cascade reactions and with tandem catalyst (Ma and Porosoff, 2019; Wei et al., 2021), have the attraction of lower equipment cost and higher CO_2 conversion. The thermodynamic equilibrium of methanol synthesis is displaced by the in situ conversion of oxygenates into hydrocarbons, which allows the integrated process to be carried out at higher temperatures and at moderate pressure (15–30 bar) compared with the conventional methanol synthesis. It is remarkable that this facilitates the supply of H_2, using commercial PEM electrolyzers.

The CO_2 hydrogenation route with oxygenates as intermediates is more attractive than the MFT reaction (based on Fe and Co catalysts) for the selective production of hydrocarbons, as it is not conditioned by the Anderson-Schulz-Flory (ASF) distribution. Using appropriate zeolites (SAPO-34, HZSM-5, Hbeta or HY, the most studied), the oxygenate

* Corresponding author.
E-mail address: ainara.ateka@ehu.eus (A. Ateka).

https://doi.org/10.1016/j.jenvman.2022.115329
Received 10 March 2022; Received in revised form 10 May 2022; Accepted 14 May 2022
Available online 21 May 2022

intermediate route can be selectively addressed towards the production of olefins, aromatics or gasoline. The acidity and appropriate shape selectivity are key features of the catalyst for this purpose (Ramirez et al., 2019; Wei et al., 2017). Comparing the deactivation of the catalysts used in oxygenates conversion into olefins, that is, MTO (methanol to olefins) and DTO (DME to olefins) processes, the high partial pressure of H_2 in the integrated CO_2 to olefins process contributes to minimizing the formation of coke on the acid catalyst (Nieskens et al., 2018), which is a relevant feature that conditions the feasibility of the overall process and the configuration of the reaction equipment (Cordero-Lanzac et al., 2020b; Tian et al., 2015).

Although conventional Cu based catalysts (with of Cu/Zn, Cu–ZnO–Al_2O_3, Cu–ZrO_2 and Cu–ZnO–ZrO_2 configurations, among others), are very active and selective for the synthesis of methanol from syngas, in the hydrogenation of CO_2 (with high H_2O concentration in the medium) and especially in the conditions required for the synthesis of hydrocarbons (above 300 °C), suffer severe deactivation by sintering and are particularly active for the rWGS reaction (Marcos et al., 2022). The adequate activity of In_2O_3 for the synthesis of methanol under these conditions, especially from pure CO_2 source, is accepted in the literature (Araújo et al., 2021a; Martin et al., 2016). Numerous experimental and theoretical studies delve into the reaction mechanism of In_2O_3, whose activity is attributed to its CO_2 adsorption capacity in the superficial oxygen vacancies and H_2 dissociation (Frei et al., 2018; Wang et al., 2021; Ye et al., 2013), favoring the advance of the reaction mechanism with formate ions as intermediates (Chen et al., 2019). CO_2 is successively hydrogenated: CO_2* → HCOO* (formate) → H_2COO* (dioxymethylene) → H_3CO* (methoxy) → CH_3OH (Chen et al., 2019; Gao et al., 2017; Ye et al., 2013, 2014).

However, at the temperature required for the direct synthesis of hydrocarbons as well, In_2O_3 presents limitations due to: i) Thermodynamics, because secondary endothermic reactions (rWGS and methanation) are favored; ii) partial sintering, favored by the required higher temperature and the presence of H_2O and CO (Wang et al., 2021). To increase the hydrogenation activity and the selectivity to methanol of In_2O_3, and reduce sintering deactivation, different strategies have been used (Wang et al., 2021): i) Improving the dispersion of In_2O_3 and increasing the oxygen vacancies, ii) promoting the dissociative H_2 adsorption and spillover; iii) promoting the activation of CO_2; iv) stabilizing key reaction intermediates, and v) generating new types of active sites.

In these strategies, the use of supports and promoters has been of great importance. From studies on the synthesis of methanol (Araújo et al., 2021a; Zhang et al., 2018) and olefins in one stage (Gao et al., 2018), the role of ZrO_2 as carrier in favoring the dispersion of In_2O_3 and generating new vacancies by the formation of epitaxially-grown In_2O_3 or solid In_2O_3–ZrO_2 solutions is well established (Nieskens et al., 2018; Ramirez et al., 2019), with the consequent increase in the adsorption capacity of CO_2 and to attenuate the sintering of In_2O_3 (Alabdullah et al., 2020; Garba et al., 2021). Additionally, In_2O_3 can be combined with other metals, active for hydrogenation reactions, such as Zn (Palos et al., 2021), Ni (Araújo et al., 2021b; Jia et al., 2020), Co (Bavykina et al., 2019; Pustovarenko et al., 2020), Au (Rui et al., 2020), Rh (Li et al., 2020), Pt (Han et al., 2021) or Pd (Araújo et al., 2021b; Frei et al., 2018; Snider et al., 2019), to increase CO_2 conversion and methanol selectivity. Various studies in the literature compare In_2O_3 based catalysts either for methanol production from syngas (Su et al., 2018) or by CO_2 hydrogenation, nonetheless, the literature studying the joint hydrogenation on CO_2+CO mixtures is scarce (Araújo et al., 2021b). The co-feeding of syngas together with CO_2 is interesting from various perspectives: i) It allows the joint valorization (avoiding separation costs) of streams derived from the gasification of biomass or wastes of the consumer society (where CO_2 and syngas are present) (Couto et al., 2013; Lopez et al., 2015), ii) considers the real need to recirculate the stream of unreacted gases in the synthesis of methanol and direct synthesis of olefins (Araújo et al., 2021b), and; iii) contributes to the necessary supply of H_2. Araújo et al. (2021a) have verified the capacity of different catalysts (In_2O_3–ZrO_2, Cu–ZnO–Al_2O_3 and ZnO–ZrO_2) for the hydrogenation of mixtures of CO and CO_2, under suitable conditions for the synthesis of methanol, verifying the favorable effect of the presence of CO on the controlled formation of surplus oxygen vacancies in In_2O_3. However, the effect on the yield and selectivity of methanol and on the deactivation of the catalyst by sintering is complex, since CO acts as a reducing agent (which favors the sintering of In_2O_3 by over-reduction). Another factor influencing the deactivation of the In_2O_3 catalyst for these feedstocks is the concentration of H_2O, which increases as CO_2 conversion increases. Several authors (Frei et al., 2018; Ye et al., 2014) have verified in the synthesis of methanol that a limited concentration of H_2O favors the formation of methoxy ions, increasing the yield of methanol. However, an excess of H_2O leads to annihilate the oxygen vacancies, to the aggregation of In species, and decrease of In^0 species, affecting the dissociation capacity of H_2, and so, the overall performance of the catalyst for CO_2 hydrogenation.

The aforementioned results in the literature show the need to progress in the knowledge and improvement of catalysts for the synthesis of methanol from CO_2 under the reaction conditions required for the integrated process (CO_2 to hydrocarbons), and especially when CO is co-fed given the interplay of CO/H_2O. The reaction conditions for maximizing CO_2 conversion and hydrocarbon production while limiting catalyst deactivation by sintering must also be optimized, since the CO_2 to hydrocarbons process is conducted at a higher temperature than the individual stage of methanol formation and at higher concentration of H_2 than oxygenates to hydrocarbons conversion. As to contribute filling this shortage, in this work, the effect of the Zr/In ratio on the In_2O_3–ZrO_2 catalyst has been studied in the synthesis of methanol from CO_2/syngas mixtures. Moreover, the selected In_2O_3–ZrO_2 catalyst (based on its good kinetic performance) has been used to conform a In_2O_3–ZrO_2/SAPO-34 tandem catalyst, and its performance has been further studied (in terms activity-selectivity-stability) in the direct synthesis of olefins. SAPO-34 has been selected (Dang et al., 2019) as acid catalyst for this purpose due to its well-known suitable behavior (highly selective) in the conversion of methanol (and/or DME) into olefins. The results are explained according to the properties of the catalysts determined by different analysis techniques.

2. Experimental

2.1. Catalyst preparation

The In_2O_3–ZrO_2 catalysts have been synthesized following a co-precipitation method (Sánchez-Contador et al., 2018). Metal nitrates solutions, $In(NO_3)_3$ (Sigma-Aldrich) and $Zr(NO_3)_4$ (Panreac) with the desired Zr/In atomic ratio (0 (In_2O_3), 1:3, 1:2, 1:1, and ZrO_2) and total metal concentration of 1 M were co-precipitated over 20 mL of deionized water under stirring, with ammonium carbonate (Panreac, 1M), at 70 °C and neutral pH. The mixtures were aged for 2 h to ensure the complete co-precipitation, and then filtered and cleaned with deionized water until neutral supernate was obtained. Finally, the resulting powders were dried and calcined at 500 °C for 1 h and pelletized, crushed and sieved to the desired particle size (125–250 μm).

SAPO-34 acid catalyst (ACS Material) was calcined at 550 °C for 5 h, pelletized, crushed and sieved to the desired particle size (300–450 μm). The tandem catalyst was composed by physical mixture of pelletized In_2O_3–ZrO_2 metallic catalyst and SAPO-34 acid catalyst in a 2/1 mass ratio. The different particle size of both functions allowed analyzing the spent catalysts independently.

2.2. Catalyst characterization

The physical properties of the catalysts (BET specific surface area and pore volume) have been determined by N_2 temperature programmed adsorption-desorption (N_2-TPD) analyses (Micromeritics ASAP 2010) at

−196 °C. The procedure consists on a previous conditioning stage of the sample, on which degassing is carried out at 150 °C under vacuum (10^{-3} mmHg) for 8 h to eliminate impurities and remove the H_2O adsorbed on the surface of the catalyst sample, facilitating N_2 sorption. Subsequently, serial equilibrium stages of N_2 adsorption-desorption are carried out until the complete saturation of the sample at cryogenic temperature of liquid N_2. The pore volume is calculated with the BJH method using the adsorption branch of the isotherm.

The chemical composition has been quantified and qualified by X-Ray fluorescence (PANalyticalAxios) and the structure by means of X-Ray diffraction (PANalyticalXpert PRO) and XRD vs temperature analyses. For determining the metallic properties, H_2 temperature programmed reduction (H_2-TPR) and CO-TPR analyses were carried out (MicromeriticsAutochem 2920). Briefly, 100 mg of sample were first swept with He to eliminate impurities and adsorbed H_2O. After stabilizing the catalyst in the corresponding mixture (10% H_2 or CO, in Ar), the samples were heated up to 800 °C at a 2 °C min^{-1} rate, and reference and analyzed streams were compared.

The same equipment was used for CO_2-TPD analyses and for acidity measurements (TPD-NH_3). For CO_2-TPD the following steps were used: i) 30 min of He sweeping (160 mL min^{-1}) at 550 °C, for eliminating possible impurities and adsorbed H_2O; ii) stabilization at 150 °C with He (20 mL min^{-1}); iii) sample saturation by CO_2 injection (5 mL min^{-1}) at 50 °C; iv) He sweeping (20 mL min^{-1}) to remove the physisorbed adsorbate; and, v) desorption by heating the sample with a controlled temperature ramp (5 °C min^{-1}) from 50 to 400 °C, the operating reaction temperature.

Analogous technique was used for NH_3-TPD analyses, using 50 μL min^{-1} NH_3 injections at 150 °C for the saturation of the sample and 5 °C min^{-1} temperature ramp for the desorption step, up to 550 °C.

2.3. Reaction equipment, conditions and indices

The reaction runs have been carried out in an isothermal PID Eng&Tech fixed bed reactor. The reactor dimensions are: 9 mm internal diameter and 10 cm of effective length and is made of 316 stainless steel. The equipment can operate up to 700 °C, 100 bar and with catalyst loadings up to 5 g. The catalyst was mixed with an inert (SiC) to ensure isothermal conditions and to avoid preferential pathways. The reactor outlet stream was heated up to 110 °C to avoid products condensation, and analyzed online in a gas-chromatograph (microGC Varian CP4900). For this analysis three modules were used: i) Molecular sieve (MS-5) to quantify H_2, N_2, O_2 and CO; ii) Porapak Q (PPQ) for CO_2, water, C_1–C_4 hydrocarbons and MeOH/DME; and iii) 5CB column (CPSiL) for higher hydrocarbons. Typically, the reaction runs were carried out at 400 °C, 30 bar, H_2/CO_X ratio of 3 and with 125 mg of catalyst. These conditions were established in a previous work as suitable for the joint valorization of CO_2 and syngas into olefins (Gao et al., 2018; Portillo et al., 2021). H_2, CO and CO_2 flowrates were adjusted to get a 3.35 g_{cat} h mol_C^{-1} space-time value with the corresponding CO_2/CO_X ratio (between 0, corresponding to 100% CO; and 1, corresponding to 100% of CO_2). The reaction system has been described in more detail elsewhere (Portillo et al., 2021).

In order to quantify the obtained results, the following reaction indices have been defined. The conversion of CO and CO_2:

$$X_{CO_x} = \frac{F^0_{CO_x} - F_{CO_x}}{F^0_{CO_x}} \cdot 100 \quad (1)$$

where $F^0_{CO_x}$ is inlet molar flowrate in content C atoms, and F_{CO_x} its analogous at the reactor outlet stream.

Similarly, CO_2 conversion, X_{CO_2} has been defined as:

$$X_{CO_2} = \frac{F^0_{CO_2} - F_{CO_2}}{F^0_{CO_2}} \cdot 100 \quad (2)$$

where $F^0_{CO_2}$ and F_{CO_2} are the CO_2 molar flowrates at the inlet and outlet of the reactor, respectively. Carbonaceous products yields (Y_i) and selectivities (S_i) (except for CO and CO_2) have been defined according to Eqs. (3) and (4), respectively, by grouping the products into the following lumps: methane, C_2–C_4 olefins, C_2–C_4 paraffins, oxygenates (MeOH and DME) by the use of the following expressions:

$$Y_i = \frac{n_i \cdot F_i}{F^0_{CO_x}} \cdot 100 \quad (3)$$

$$S_i = \frac{n_i \cdot F_i}{\sum_i (n_i \cdot F_i)} \cdot 100 \quad (4)$$

being n_i the number of C atoms in a molecule of component i and F_i the molar flowrate of the component i at the reactor outlet stream.

The carbon balance in all experiments was closed over 99%.

3. Results and discussion

In this section, first, the effect of the Zr loading on the properties of the In_2O_3–ZrO_2 catalyst has been studied. Second, a comparison of the performance of the catalysts for CO_2/CO mixtures hydrogenation has been carried out in order to select the most suitable Zr/In ratio to favor methanol production. The reaction runs have been carried out under the reaction conditions required for the direct olefins synthesis process, pursuing to use the selected In_2O_3–ZrO_2 catalyst in a In_2O_3–ZrO_2/SAPO-34 tandem for this reaction. Catalyst screening has been carried out attending to activity, selectivity to methanol and stability criteria. Finally, the performance of the In_2O_3–ZrO_2/SAPO-34 tandem catalyst has been assessed for the direct synthesis of olefins from CO_2/CO mixtures.

3.1. Effect of the Zr loading in the properties of the metallic catalyst

Attending to the physical properties of the catalysts (Table 1) determined by N_2-TPD analyses, the pore volume of In_2O_3 is higher (0.25 cm^3 g^{-1}) than that of ZrO_2 (0.16 cm^3 g^{-1}). Consequently, the pore volume of the composite In_2O_3–ZrO_2 catalysts decreases with increasing Zr loading in the catalyst. As to the BET specific surface area (S_{BET}) regards, being 53 m^2 g^{-1} for In_2O_3 and 96 m^2 g^{-1} for ZrO_2, the S_{BET} of In_2O_3–ZrO_2 catalysts increases upon increasing Zr/In ratio, in agreement with the results reported by Frei et al. (2020). Indeed, higher S_{BET} than expected from the Zr/In ratio has been obtained for the In_2O_3–ZrO_2 catalysts.

As to the chemical and metallic properties characterization regards, XRF analyses have been carried out to ascertain the co-precipitation of the metals in the desired Zr/In ratio. In Table 2, the nominal and measured metal ratios are listed.

As to analyze the morphology of the catalysts, XRD patterns for the different catalysts are depicted in Fig. 1. According to these spectra, pure In_2O_3 and ZrO_2 catalysts show the typical peaks for these structures. At 2 θ = 21.68°, 30.74°, 35.61°, 37.88°, 40°, 42.03°, 43.99°, 45.86,° 51.14°, 52.84°, 56.14°, 59.245°, 60.784°, 62.33° and 63.79° for In_2O_3, and; at 2 θ = 30.6876°, 35.5315°, 51.0336°, 60.6445°, 63.0967°, 74.9399° for ZrO_2. For the composite catalysts, that is, for the mixture of In_2O_3 with ZrO_2, a combination of those in good agreement with the Zr/In ratio reported in Table 2 is observed. Moreover, the results evidence that ZrO_2

Table 1
Effect of Zr/In ratio over catalyst physical properties.

Catalyst	S_{BET} (m^2 g^{-1})	V_p (cm^3 g^{-1})
In_2O_3	53	0.25
1Zr–3In	85	0.23
1Zr-2In	86	0.23
1Zr–1In	95	0.17
ZrO_2	96	0.16

Table 2
Nominal and measured Zr/In ratios.

	Nominal	Measured
In_2O_3	0	0
1Zr–3In	1/3	1/3.11
1Zr–2In	1/2	1/1.98
1Zr–1In	1/1	1/0.90
ZrO_2	Inf.	Inf.

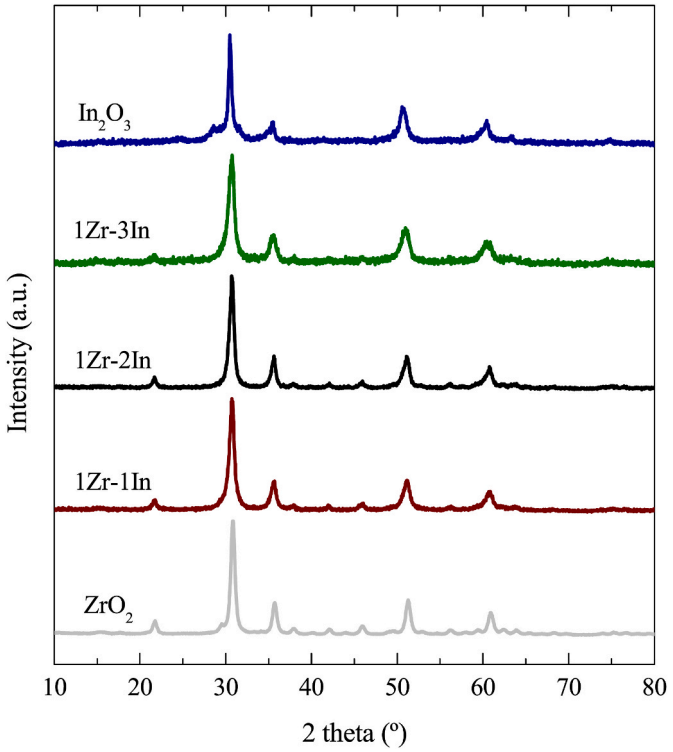

Fig. 1. XRD patterns for the In_2O_3–ZrO_2 catalysts with different Zr/In ratio.

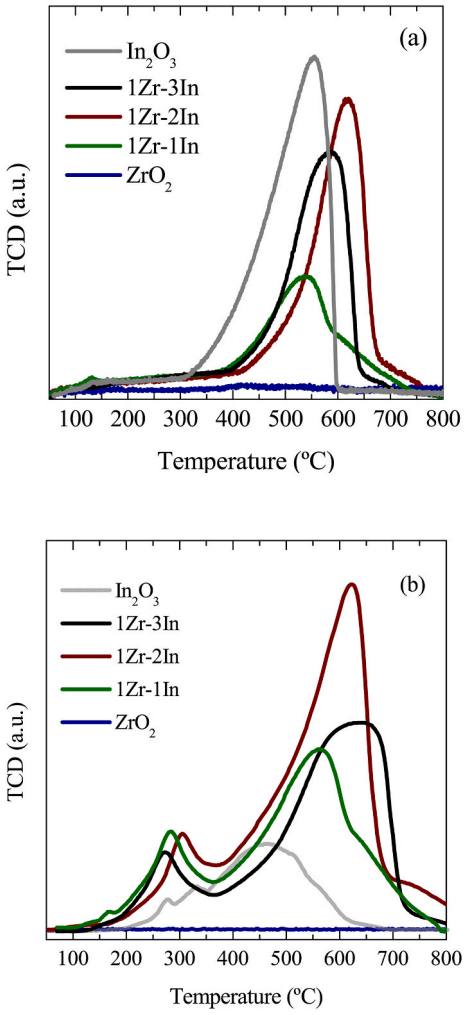

Fig. 2. Effect of Zr/In ratio on catalyst reducibility using H_2 (a) or CO (b) as reducing agent.

coexists in its monoclinic (most favored thermodynamically) (Martin et al., 2016) and tetragonal structure, whereas it changes completely into its tetragonal polymorph with the incorporation of In_2O_3 in the In_2O_3–ZrO_2 catalysts as determined in the literature (Frei et al., 2019). Moreover, from further XRD vs temperature measurements carried out, the structure of the In_2O_3–ZrO_2 catalysts is expected to remain stable under the reaction temperatures used in the direct CO_2/syngas to olefins process. Additionally, the Rietveld calculations carried out evidenced the presence of Zr atoms in the In_2O_3 structure and of In atoms integrated in the ZrO_2 structure, which is consistent with previous findings (Artamonova et al., 2006; Frei et al., 2020; Portillo et al., 2021). For the 1Zr–1In catalyst, 42.6% of In_2O_3 structure and 57.4% of ZrO_2 structures were determined. The metal content within the In_2O_3 structure, is divided into 81.2% of In, and 18.8% of Zr. Likewise, within in the ZrO_2 structure, 76.2% stands for Zr and 23.8% for In. These results are consistent with the suggestion in the literature that indium-zirconium composite oxides are not simple mechanical mixtures but generate active composite $In_{1-x}Zr_xO_y$ oxides (Dang et al., 2018).

The reducibility of the catalysts has been studied by H_2-TPR and CO-TPR analyses (Fig. 2, where the TCD signals have been normalized for In_2O_3 mass). With this approach, gathering information on the H_2 splitting activity (H_2 desorption) and on the reducibility of the catalyst in the reaction medium is pursued. Prior to both H_2 and CO-TPR, the samples were swept with He at 200 °C for 1 h to eliminate impurities and adsorbed water. Later on, the samples were cooled down to 30 °C, the inlet gas changed to H_2/CO and temperature increased after attaining a stable baseline at 30 °C.

As expected, ZrO_2 is not reduced under the studied TPR conditions and so, it is not expected either under the not so severe reaction temperature used. As observed, the combination of In_2O_3 and ZrO_2 incurs peaks at higher temperatures for In_2O_3–ZrO_2 catalyst compared to In_2O_3 and ZrO_2, for both reducing agents. Comparing H_2-TPR (Fig. 2a) and CO-TPR (Fig. 2b), CO presents higher reduction capacity, which is in accordance with the previous results (Chen et al., 2019; Dang et al., 2018; Frei et al., 2018; Martin et al., 2016). The results also indicate a favorable effect of the addition of ZrO_2 on the number of In_2O_3 sites accessible to H_2 and CO (greater area under the curve per unit mass of In_2O_3). It is noteworthy that the presence of ZrO_2 favors the reduction of In_2O_3 with CO at low temperature, as a peak is observed with a maximum between 275 and 300 °C for composite In_2O_3–ZrO_2 catalysts. The effect of CO as vacancy generator (Martin et al., 2016; Wang et al., 2021) will contribute to this result, also favoring its adsorption and that of CO_2.

Fig. 2 also shows a greater resistance to reduction of In_2O_3 sites due to the presence of ZrO_2. This lower reducibility is consistent with the larger crystal size of In_2O_3 observed with increasing Zr/In ratio (Table 3). In addition, it is well established in the literature that the presence of ZrO_2 hinders the sintering of In_2O_3 (Araújo et al., 2021b), which is consistent with the lower reducibility observed in Fig. 2 for moderate ZrO_2 contents in the composite catalyst.

CO_2-TPD analysis have been carried out for all the catalysts to quantify their CO_2 adsorption capacity, since this is a key feature for

Table 3
Effect of Zr/In ratio in the catalyst on the average size of the crystals in the In_2O_3–ZrO_2 composites.

Catalyst	Crystal size (nm)	
In_2O_3	17.3	In_2O_3
	–	ZrO_2
1Zr–3In	17.6	In_2O_3
	5.5	ZrO_2
1Zr–2In	21	In_2O_3
	8	ZrO_2
1Zr–1In	11.5	In_2O_3
	11.5	ZrO_2
ZrO_2	–	In_2O_3
	10.8	ZrO_2

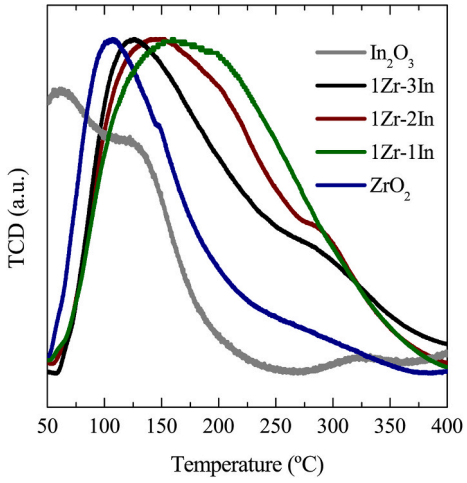

Fig. 3. CO_2-TPD profiles for the In_2O_3–ZrO_2 catalysts with different Zr loading.

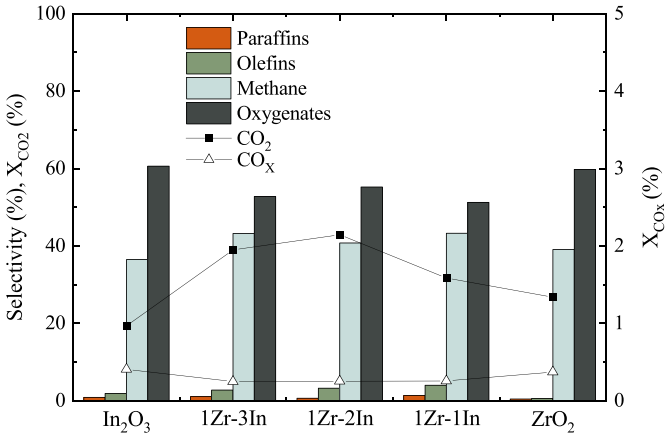

Fig. 4. Conversion and selectivities for In_2O_3–ZrO_2 catalysts with different Zr/In ratios. Operating conditions: 400 °C; 30 bar; H_2/CO_2, 3; CO_2/CO_X, 1; space time, 3.35 g_{cat} h mol_C^{-1}; TOS 5 h.

their activity for oxygenates synthesis. The results are plotted in Fig. 3. According to these profiles, In_2O_3–ZrO_2 catalysts outperform significantly the CO_2 adsorption capacity of the parent In_2O_3 and ZrO_2 catalysts.

The responsibility of the oxygen vacancies in In_2O_3 on the CO_2 adsorption capacity and activity for hydrogenation to methanol is well

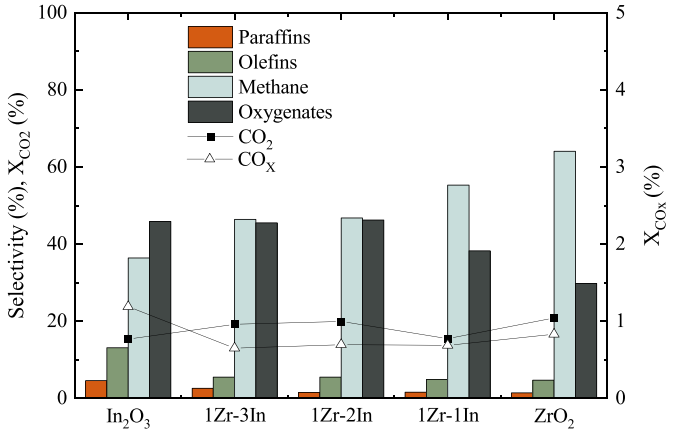

Fig. 5. Conversion and selectivities for In_2O_3–ZrO_2 catalysts with different Zr/In ratios. Operating conditions: 400 °C; 30 bar; H_2/CO_X, 3; CO_2/CO_X, 0.5; space time, 3.35 g_{cat} h mol_C^{-1}; TOS 5 h.

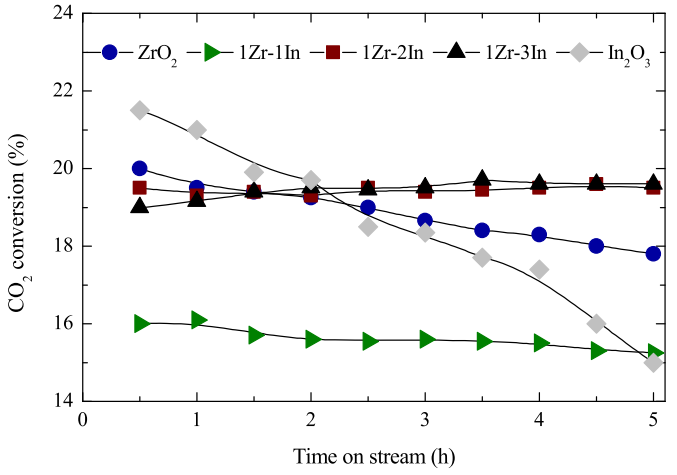

Fig. 6. Evolution of CO_2 conversion with TOS for In_2O_3–ZrO_2 catalysts with different Zr/In ratios. Operating conditions: 400 °C; 30 bar; H_2/CO_X, 3; CO_2/CO_X, 0.5; space time, 3.35 g_{cat}h mol_C^{-1}.

established (Martin et al., 2016; Sun et al., 2015). Consequently, the higher CO_2 adsorption capacity of the In_2O_3–ZrO_2 catalyst than of In_2O_3 observed in Fig. 6 is attributable to its higher density of oxygen vacancies. Dang et al. (2018) determine by X-ray photoelectron spectroscopy (XPS), CO_2-TPD analysis, and periodic DFT calculations that the incorporation of ZrO_2 into In_2O_3 generates interactions in the electronic structure, the formation of $In_{1-x}Zr_xO_y$ mixed oxide and the formation of additional oxygen vacancies, increasing CO_2 conversion.

Regarding the characterization of the SAPO-34 acid function: an specific surface area BET of 652 $^{m2g-1}$, micropore volume of 0.2192 cm^3 g^{-1}, and total pore volume of 0.23 cm^2 g^{-1}were determined (Fig. S1). In the NH_3-TPD analysis (Fig. S2) 777.6 $mmol_{NH3}$ g_{cat}^{-1} were measured for SAPO-34, and from the profile two types of acid sites were identified, with peaks at 180 °C (14%) and 375 °C (86%), related to weak and strong acid sites, respectively.

3.2. *Effect of the Zr loading in the performance of the catalyst for methanol synthesis*

The performance of the In_2O_3–ZrO_2 catalysts has been studied in CO_2

(Fig. 4) and CO_2/CO mixtures hydrogenation (Fig. 5) under the reaction conditions (described in Section 2.3). It is observed in Fig. 4, that for CO_2 hydrogenation, parent catalysts (thus, In_2O_3 and ZrO_2) reach slightly higher CO_X conversion values than combined metal oxides, and even higher oxygenates selectivities. However, all CO_2 conversion values are significantly enhanced in the In_2O_3–ZrO_2 catalysts. For the catalysts with a Zr/In ratio of 1/3 and 1/2 similar performance is observed, thus, more than doubling the value of X_{CO2} with respect to that obtained with In_2O_3 and upgrading that of ZrO_2 over 50–60%. However, the selectivity of oxygenates decreases from 60% to 55% for In_2O_3–ZrO_2 catalysts, as a consequence of the increase in the formation of methane and, to a lesser extent, of olefins. It should be noted that the results in Fig. 6 evidence that the weakly acidic sites (Lewis sites) of ZrO_2 in the In_2O_3–ZrO_2 catalysts (Dang et al., 2018) are sufficient to activate the dual cycle mechanism, with a reduced conversion of methanol into olefins, justifying the upturning olefins yield when increasing the Zr content. However, ZrO_2 itself is not sufficient for the formation of olefins, because the presence of In_2O_3 is required for an efficient CO_2 adsorption and H_2 splitting as the first steps for methanol formation.

Based on these results, a Zr/In ratio in the range between 1/3 and 1/2 is considered adequate to maximize both pursued targets in the hydrogenation of CO_2, thus, CO_2 conversion and oxygenate yield. This upgrade in CO_2 conversion for the In_2O_3–ZrO_2 catalysts at 400 °C is consistent with the characterization results observed in the H_2-TPR (Fig. 2a) and CO_2-TPD of (Fig. 3) analyses. Both results explain the synergy in the conversion of CO_2 by the improvement of the CO_2 adsorption capacity by ZrO_2 and H_2 dissociation on In_2O_3 sites, due to the proximity of these sites. Frei et al. (2020) already observed this phenomenon in the usual conditions of methanol synthesis from CO_2 (300 °C) with In_2O_3–ZrO_2 catalysts.

Comparing the results in Figs. 4 and 5, a significant effect of the feed composition over the performance of the catalysts is evidenced. In both cases, the high CH_4 selectivity is noteworthy, being higher for CO_2/CO mixture hydrogenation (Fig. 5). For this feed, higher Zr/In ratio in the tandem catalysts leads to upturn CH_4 selectivity, at the expense of olefins and oxygenates yields. This significant CH_4 formation, is consequence of the fact that the endothermic methanation reaction is favored at such high reaction temperature of 400 °C required in the direct CO_2 to olefins process. However, this reaction, which also occurs with methoxy ions as intermediates, as oxygenates formation does (Solis-Garcia et al., 2017), will be suppressed in the direct synthesis of olefins, by the in situ conversion of these ions into olefins, by means of the very fast dual cycle mechanism over the SAPO-34 catalyst (Cordero-Lanzac et al., 2020a) (subsequent section 3.4). The greater CO_2 conversion attained with the catalyst with Zr/In ratio of 1/2 (Fig. 4) is interesting for its use in the direct synthesis of olefins by CO_2 and CO_2/CO hydrogenation.

For further studying the effect that adding ZrO_2 might have in the deactivation of In_2O_3–ZrO_2 catalysts, the evolution of CO_2 conversion with time on stream is compared in Fig. 6 for CO_2/CO mixture hydrogenation. It is noticeable that deactivation is only observed for pure In_2O_3. These trends evidence that ZrO_2 addition improves the stability of the parent In_2O_3 catalyst. In accordance with the results in Figs. 4 and 5, 1Zr–2In and 1Zr–3In catalysts have also similar performance for the evolution of CO_2 conversion with time on stream.

This high stability of the catalyst in presence of ZrO_2 is also evident in the evolution of products distribution with time on stream for the tested 24 h. As an example, in Fig. 7, the evolution of products yield with time on stream is depicted for the In_2O_3–ZrO_2 catalyst with Zr/In of 1/2 for the hydrogenation of a CO_2/CO mixture with a CO_2/CO_X ratio of 0.5.

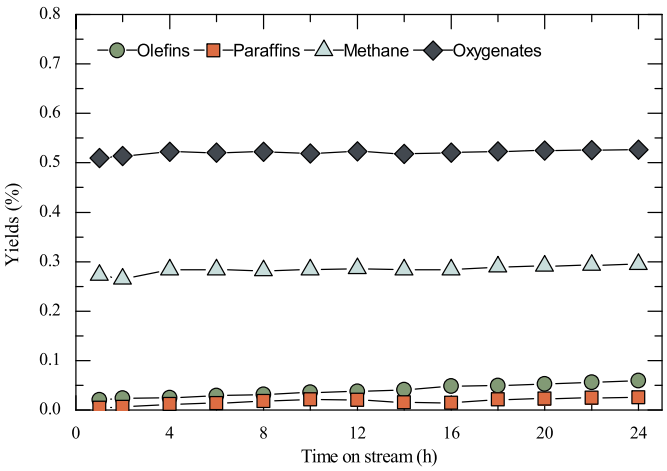

Fig. 7. Evolution of products yields with time on stream for In_2O_3–ZrO_2 catalyst with Zr/In of 1/2. Operating conditions: 400 °C; 30 bar; H_2/CO_X, 3; CO_2/CO_X, 0.5; space time, 3.35 $g_{cat}h\ mol_C^{-1}$.

A high CO_2 conversion with ZrO_2 catalyst is also observed in Fig. 6. However, this result is a consequence of an undesired high CH_4 formation (Fig. 5). In addition, Figs. 4–6 show that for a Zr/In ratio of 1/1 the conversion of CO_2 is remarkably lower, which does not correspond to the CO_2 adsorption capacity (Fig. 3). This result is explained because with this Zr/In ratio the amount of In_2O_3 is not enough for the dissociation of the H_2 amount required for the methanol and CH_4 formation reactions.

All in all, considering CO_2 conversion, oxygenates selectivity, catalyst stability and the influence of the CO_2/CO composition in the feed, the composite catalyst with Zr/In ratio of 1/2 is considered to give the best balanced results, and so, the best prospects for conforming tandem In_2O_3–ZrO_2/SAPO-34 catalysts for the direct olefins synthesis.

3.3. *Effect of CO_2/CO_X composition in the feed on product distribution*

As it is sensed by comparing the results in Figs. 4 and 5, the composition of the CO_2/CO_X mixture in the feed has a great effect on products distribution in the synthesis of methanol using In_2O_3–ZrO_2 catalysts. In Fig. 8, product yield values after 16 h TOS corresponding to the catalysts with Zr/In ratios of 1/2 (Figs. 8a) and 1/3 (Fig. 8b) are shown. It is observed that in both cases CH_4 formation decays sharply when co-feeding CO_2 together with syngas. It is also noteworthy that methanol yield passes through a maximum for feed compositions with equal concentration of CO and CO_2. Likewise, the results in Fig. 8b contribute to further standing out the greater production of methane the 1Zr–3In catalyst leads to, being it especially relevant for pure syngas feeds (CO_2/CO_X, 0). Probably due to the over-reduction of the catalyst, in good agreement with the highest reducibility under H_2 and CO atmospheres reported in section 3.1.

Accordingly, these results reaffirm the selection of 1Zr–2In as the In_2O_3–ZrO_2 catalyst with best prospects to be used in combination with SAPO-34 in the direct olefins formation from CO_2 and syngas mixtures whatever CO_2/CO composition.

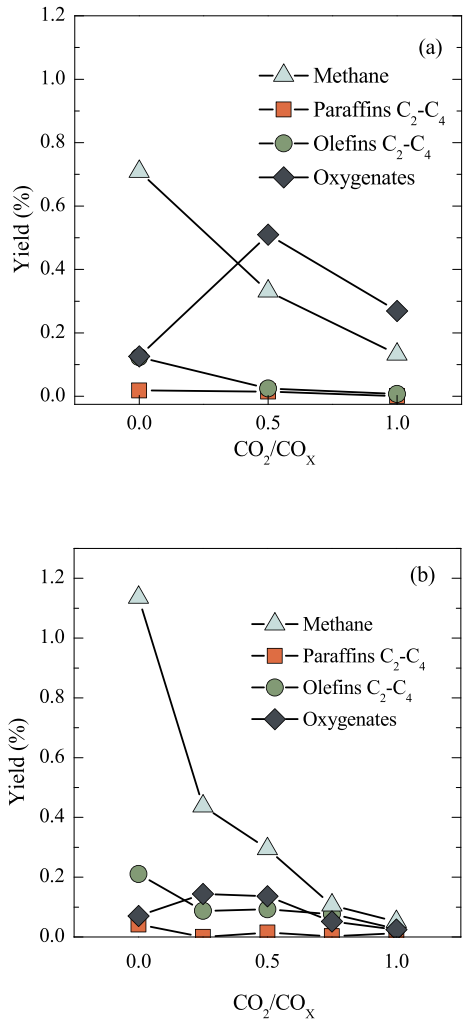

Fig. 8. Effect of the CO_2/CO_X composition in the feed over products yield for methanol synthesis for In_2O_3–ZrO_2 catalyst with Zr/In ratio of 1/2 (a) and 1/3 (b). Operating conditions: 400 °C; 30 bar; H_2/CO_X, 3; space time, 3.35 g_{cat} h mol_C^{-1}; TOS 5 h.

3.4. *Kinetic performance of the tandem In_2O_3–ZrO_2/SAPO-34 catalyst in the hydrogenation of CO_2/CO mixtures into olefins*

The suitability of the selected In_2O_3–ZrO_2 catalyst (1Zr–2In) in the direct synthesis of olefins process has been addressed in this section. Fig. 9 illustrates the products yields obtained with the tandem In_2O_3–ZrO_2/SAPO-34 catalyst for feeds with different composition. The results evidence the good performance of the tandem catalyst, given almost all the oxygenated compounds formed as intermediates are converted into hydrocarbons, the selectively to olefins, being paraffins the only by-products, and the absence of CH_4.

Comparing the results of the direct synthesis of olefins (Fig. 9) with those in Fig. 8 of the first stage of the process (oxygenates formation), various features are to be highlighted: i) The upgrade of the overall conversion obtained in the direct synthesis. Thus, CO_X conversion increases from 0.88% to 4.28% for feeds with CO_2/CO_X ratio of 0.5, and the conversion of the targeted products from 0.51% (oxygenates yield in methanol formation) to 3.11% (olefins yield). ii) The suppression of the undesired methane formation pathway, being it almost undetectable.

The mechanism of hydrocarbon formation directly by hydrogenation of CO_2 and CO on the In_2O_3–ZrO_2/SAPO-34 tandem catalyst is the cascade combination of the mechanisms of methanol/DME synthesis and the in situ conversion of these oxygenates into hydrocarbons. It is

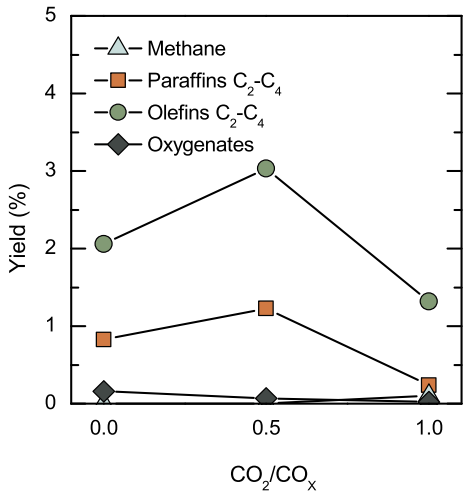

Fig. 9. Effect of the CO_2/CO_X composition in the feed over products yield in the direct synthesis of olefins with In_2O_3–ZrO_2/SAPO-34 catalyst of Zr/In ratio of 1/2. Operating conditions: 400 °C; 30 bar; H_2/CO_X, 3; space time, 5 g_{cat} h mol_C^{-1}; TOS 24 h.

well established in the literature (Frei et al., 2018; Tan et al., 2019; Ye et al., 2012, 2013) that in methanol synthesis over In_2O_3–ZrO_2 catalysts, CO_2 is adsorbed on In_2O_3 oxygen vacancies and on additional oxygen vacancies formed by the presence of ZrO_2 and the formation of stable $In_{1-x}ZrO_xO_y$ mixed oxide. The H_2 dissociation capacity of the In_2O_3 in In_2O_3–ZrO_2 facilitates the hydrogenation of adsorbed CO_2 to form formate species (HCOO*). The next steps consists of the reaction of these species with H* ions to produce H_2COO* species, and the hydrogenation of the latter to methoxy species (H_3CO*), which will hydrogenate to form methanol. The presence of these intermediates has been determined by means of experimental and theoretical studies (Dang et al., 2018; Wang et al., 2021). The effect of the presence of CO in this reaction mechanism is controversial. Besides disfavoring the rWGS reaction, it is well established (Martin et al., 2016) that a moderate concentration of CO increases the density of oxygen vacancies, favoring therefore CO_2 adsorption and the extent of methanol formation. However, due to its strong reducing character (verified in Fig. 2b), a high concentration of CO can favor the over-reduction of In_2O_3 and its sintering (Araújo et al., 2021b). The results in Fig. 9 are consistent with the commented effect of CO concentration, giving rise to higher olefins yield for the CO_2/CO_x ratio of 0.5 in the feed than for the hydrogenation of CO (CO_2/CO_x of 0), as a consequence of the higher methanol yield.

The formation of the C–C bonds of the light olefins from methanol/DME is a consequence of the activity of the acid sites of SAPO-34 (Gayubo et al., 2000; Pérez-Uriarte et al., 2016). The reaction proceeds through the dual cycle mechanism, with two related routes, with polyalkyl benzenes and olefins as intermediates (Gao et al., 2019). The severe shape selectivity of SAPO-34, with CHA topology (cavities of 10 × 6.7 Å connected by 3.8 × 3.8 Å 8-ring cages) (Hemelsoet et al., 2013), is suitable for the selective formation of ethylene and propylene when used in the tandem In_2O_3–ZrO_2/SAPO-34 catalyst (Dang et al., 2019; Portillo et al., 2021).

The evolution of products yield with time on stream obtained in the direct synthesis of olefins is shown in Fig. 10. These results, corresponding to the most severe deactivation conditions studied, that is, for syngas feeds, evidences that after an initial activity decay taking place in the first 4 h of reaction, an pseudo-steady state is achieved (in this case and for all the studied feed compositions). From characterization analyses through temperature programmed oxidation (TPO) with air (results not shown), this deactivation is attributed to coke deposition in the acid function (coke content of 4.9 wt% on the acid catalyst and 0.5 wt% on the metallic catalyst of the tandem catalyst, for the reaction

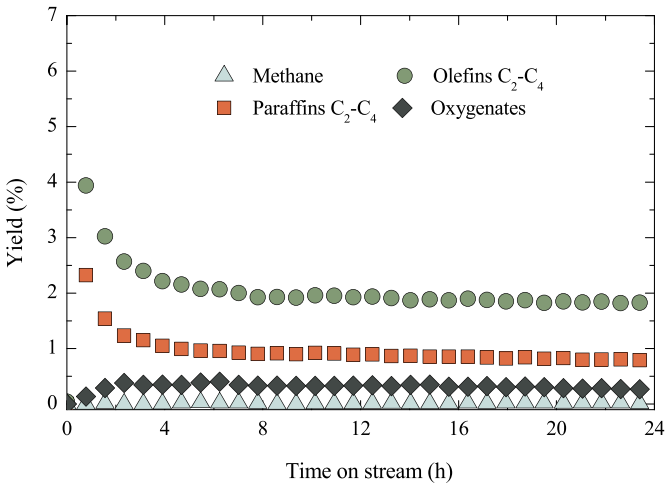

Fig. 10. Evolution of products yields with time on stream in the direct hydrogenation of CO_2/CO to olefins with In_2O_3–ZrO_2/SAPO-34 catalyst. Operating conditions: 400 °C; 30 bar; H_2/CO,3; CO_2/CO_X,0; space time, 5 $g_{cat}h\ mol_C^{-1}$.

conditions in Fig. 10). Coke formation takes place fast in the first reaction hours over SAPO-34, reaching almost the maximum reported value in 2 h TOS (4.6 wt% and 4.9 wt% at pseudo-stable conditions). Once at that point, coke formation rate is residual, suppressed by the hydrogenation of the intermediates, and does not lead to further activity decay.

4. Conclusions

The addition of Zr to In_2O_3 catalysts improves the performance (activity, oxygenates selectivity and stability) for the hydrogenation of CO_2/CO mixtures to methanol under the suitable operation conditions for the direct CO_2 to olefins process (400 °C, 30 bar). This is a key feature for the configuration of tandem catalysts for the direct conversion of CO_2 (and syngas) into olefins via the route with oxygenates as intermediates. The behavior of the In_2O_3–ZrO_2 catalysts is a consequence of its properties. The loading of ZrO_2 with a Zr/In ratio between 1/3 and 1/2 increases the yield of oxygenates compared to that obtained with parent In_2O_3 and ZrO_2 catalysts, improves stability, and is suitable for attaining an outstanding conversion co-feeding CO (syngas) together with CO_2, albeit with high formation of CH_4 (favored with increasing Zr/In ratio).

Accordingly, the In_2O_3–ZrO_2 catalyst with Zr/In of 1/2 has been selected as suitable for its use in the In_2O_3–ZrO_2/SAPO-34 tandem catalyst for the direct synthesis of olefins. The results obtained with this catalyst offer a good balance between CO_2 and CO_X conversion, olefins yield and selectivity, and catalyst stability at 400 °C and 30 bar, for different CO_2/CO_X composition feeds. The in situ conversion of the formed oxygenates into olefins, displaces the thermodynamic equilibrium of the methanol formation reactions, and as a result, olefins yield 6 folds compared to the oxygenates yield of the first stage, and methane formation is negligible.

The results (obtained at low space time values, to work in demanding conditions for the stability of the tandem catalyst) are encouraging to progress towards the optimization of the operating conditions for the joint valorization of CO_2 and syngas, which is an interesting strategy to mitigate climate change.

CRediT authorship contribution statement

A. Portillo: Conceptualization, Methodology, Investigation, Validation, Data curation, Writing – original draft, Writing – review & editing. **A. Ateka:** Conceptualization, Methodology, Investigation, Validation, Data curation, Writing – original draft, Writing – review & editing. **J. Ereña:** Data curation, Writing – original draft. **J. Bilbao:** Conceptualization, Methodology, Investigation, Data curation, Writing – original draft, Writing – review & editing, Supervision. **A.T. Aguayo:** Project administration, Conceptualization, Supervision, Validation, Data curation.

Declaration of competing interest

The authors declare that they have no known competing financial interests or personal relationships that could have appeared to influence the work reported in this paper.

Acknowledgements

This work has been carried out with the financial support of the Ministry of Science, Innovation and Universities of the Spanish Government (PID2019-108448RB-100); the Basque Government (Project IT1645-22), the European Regional Development Funds (ERDF) and the European Commission (HORIZON H2020-MSCA RISE-2018. Contract No. 823745). A. Portillo is grateful for the grateful for the Ph.D. grant from the Ministry of Science, Innovation and Universities of the Spanish Government (BES2017-081135). The authors thank for technical and human support provided by SGIker (UPV/EHU).

Appendix A. Supplementary data

Supplementary data to this article can be found online at https://doi.org/10.1016/j.jenvman.2022.115329.

References

Alabdullah, M.A., Gomez, A.R., Vittenet, J., Bendjeriou-Sedjerari, A., Xu, W., Abba, I.A., Gascon, J., 2020. A viewpoint on the refinery of the future: catalyst and process challenges. ACS Catal. 10, 8131–8140. https://doi.org/10.1021/acscatal.0c02209.

Araújo, T.P., Hergesell, A.H., Faust-Akl, D., Büchele, S., Stewart, J.A., Mondelli, C., Pérez-Ramírez, J., 2021a. Methanol synthesis by hydrogenation of hybrid CO_2—CO feeds. ChemSusChem 14, 2914–2923. https://doi.org/10.1002/CSSC.202100859.

Araújo, T.P., Shah, A., Mondelli, C., Stewart, J.A., Curulla Ferré, D., Pérez-Ramírez, J., 2021b. Impact of hybrid CO_2-CO feeds on methanol synthesis over In_2O_3-based catalysts. Appl. Catal. B Environ. 285 https://doi.org/10.1016/j.apcatb.2021.119878.

Artamonova, O.V., Almjasheva, O.V., Mittova, I.Y., Gusarov, V.V., 2006. Zirconia-based nanocrystals in the ZrO_2-In_2O_3 system. Inorg. Mater. 42, 1072–1075. https://doi.org/10.1134/S0020168506100049.

Bavykina, A., Yarulina, I., Al Abdulghani, A.J., Gevers, L., Hedhili, M.N., Miao, X., Galilea, A.R., Pustovarenko, A., Dikhtiarenko, A., Cadiau, A., Aguilar-Tapia, A., Hazemann, J.L., Kozlov, S.M., Oud-Chikh, S., Cavallo, L., Gascon, J., 2019. Turning a methanation Co catalyst into an in-Co methanol producer. ACS Catal. 9, 6910–6918. https://doi.org/10.1021/ACSCATAL.9B01638.

Chen, T.Y., Cao, C., Chen, T.B., Ding, X., Huang, H., Shen, L., Cao, X., Zhu, M., Xu, J., Gao, J., Han, Y.F., 2019. Unraveling highly tunable selectivity in CO_2 hydrogenation over bimetallic in-Zr oxide catalysts. ACS Catal. 9, 8785–8797. https://doi.org/10.1021/acscatal.9b01869.

Cordero-Lanzac, T., Aguayo, A.T., Bilbao, J., 2020a. Reactor-regenerator system for the dimethyl ether-to-olefins process over HZSM-5 catalysts: conceptual development and analysis of the process variables. Ind. Eng. Chem. Res. 59, 14689–14702. https://doi.org/10.1021/acs.iecr.0c02276.

Cordero-Lanzac, T., Martínez, C., Aguayo, A.T., Castaño, P., Bilbao, J., Corma, A., 2020b. Activation of n-pentane while prolonging HZSM-5 catalyst lifetime during its combined reaction with methanol or dimethyl ether. Catal. Today 383, 320–329. https://doi.org/10.1016/j.cattod.2020.09.015.

Couto, N., Rouboa, A., Silva, V., Monteiro, E., Bouziane, K., 2013. Influence of the biomass gasification processes on the final composition of syngas. Energy Proc. 36, 596–606. https://doi.org/10.1016/J.EGYPRO.2013.07.068.

Dang, S., Gao, P., Liu, Z., Chen, X., Yang, C., Wang, H., Zhong, L., Li, S., Sun, Y., 2018. Role of zirconium in direct CO_2 hydrogenation to lower olefins on oxide/zeolite bifunctional catalysts. J. Catal. 364, 382–393. https://doi.org/10.1016/j.jcat.2018.06.010.

Dang, S., Li, S., Yang, C., Chen, X., Li, X., Zhong, L., Gao, P., Sun, Y., 2019. Selective transformation of CO_2 and H_2 into lower olefins over In_2O_3-$ZnZrO_x$/SAPO-34 bifunctional catalysts. ChemSusChem 12, 3582–3591. https://doi.org/10.1002/cssc.201900958.

Frei, M.S., Capdevila-Cortada, M., García-Muelas, R., Mondelli, C., López, N., Stewart, J. A., Curulla Ferré, D., Pérez-Ramírez, J., 2018. Mechanism and microkinetics of methanol synthesis via CO_2 hydrogenation on indium oxide. J. Catal. 361, 313–321. https://doi.org/10.1016/j.jcat.2018.03.014.

Frei, M.S., Mondelli, C., Cesarini, A., Krumeich, F., Hauert, R., Stewart, J.A., Curulla, D., Ferré, F., Pérez-Ramírez, J., 2020. Role of Zirconia in Indium Oxide-Catalyzed CO_2 Hydrogenation to Methanol. https://doi.org/10.1021/acscatal.9b03305.

Frei, M.S., Mondelli, C., García-Muelas, R., Kley, K.S., Puértolas, B., López, N., Safonova, O.V., Stewart, J.A., Curulla Ferré, D., Pérez-Ramírez, J., 2019. Atomic-scale engineering of indium oxide promotion by palladium for methanol production via CO_2 hydrogenation. Nat. Commun. 10 https://doi.org/10.1038/S41467-019-11349-9.

Gao, M., Li, H., Yang, M., Zhou, J., Yuan, X., Tian, P., Ye, M., Liu, Z., 2019. A modeling study on reaction and diffusion in MTO process over SAPO-34 zeolites. Chem. Eng. J. 377, 119668. https://doi.org/10.1016/j.cej.2018.08.054.

Gao, P., Dang, S., Li, S., Bu, X., Liu, Z., Qiu, M., Yang, C., Wang, H., Zhong, L., Han, Y., Liu, Q., Wei, W., Sun, Y., 2018. Direct production of lower olefins from CO2 conversion via bifunctional catalysis. ACS Catal. 8, 571–578. https://doi.org/10.1021/acscatal.7b02649.

Gao, P., Li, S., Bu, X., Dang, S., Liu, Z., Wang, H., Zhong, L., Qiu, M., Yang, C., Cai, J., Wei, W., Sun, Y., 2017. Direct conversion of CO_2 into liquid fuels with high selectivity over a bifunctional catalyst. Nat. Chem. 9, 1019–1024. https://doi.org/10.1038/nchem.2794.

Garba, M.D., Usman, M., Khan, S., Shehzad, F., Galadima, A., Ehsan, M.F., Ghanem, A.S., Humayun, M., 2021. CO_2 towards fuels: a review of catalytic conversion of carbon dioxide to hydrocarbons. J. Environ. Chem. Eng. 9, 104756. https://doi.org/10.1016/J.JECE.2020.104756.

Gayubo, A.G., Aguayo, A.T., Sánchez Del Campo, A.E., Tarrío, A.M., Bilbao, J., 2000. Kinetic modeling of methanol transformation into olefins on a SAPO-34 catalyst. Ind. Eng. Chem. Res. 39, 292–300. https://doi.org/10.1021/ie990188z.

Han, Z., Tang, C., Wang, J., Li, L., Li, C., 2021. Atomically dispersed Ptn+ species as highly active sites in Pt/In2O3 catalysts for methanol synthesis from CO2 hydrogenation. J. Catal. 394, 236–244. https://doi.org/10.1016/j.jcat.2020.06.018.

Hemelsoet, K., Van Der Mynsbrugge, J., De Wispelaere, K., Waroquier, M., Van Speybroeck, V., 2013. Unraveling the reaction mechanisms governing methanol-to-olefins catalysis by theory and experiment. ChemPhysChem 14, 1526–1545. https://doi.org/10.1002/cphc.201201023.

Hepburn, C., Adlen, E., Beddington, J., Carter, E.A., Fuss, S., Mac Dowell, N., Minx, J.C., Smith, P., Williams, C.K., 2019. The technological and economic prospects for CO2 utilization and removal. Nature. https://doi.org/10.1038/s41586-019-1681-6.

Jia, X., Sun, K., Wang, J., Shen, C., Liu, C. jun, 2020. Selective hydrogenation of CO_2 to methanol over Ni/In_2O_3 catalyst. J. Energy Chem. 50, 409–415. https://doi.org/10.1016/j.jechem.2020.03.083.

Kamkeng, A.D.N., Wang, M., Hu, J., Du, W., Qian, F., 2021. Transformation technologies for CO_2 utilisation: current status, challenges and future prospects. Chem. Eng. J. 409, 128138. https://doi.org/10.1016/J.CEJ.2020.128138.

Leonzio, G., 2018. State of art and perspectives about the production of methanol, dimethyl ether and syngas by carbon dioxide hydrogenation. J. CO2 Util. 27, 326–354. https://doi.org/10.1016/j.jcou.2018.08.005.

Li, M.M.J., Zou, H., Zheng, J., Wu, T.S., Chan, T.S., Soo, Y.L., Wu, X.P., Gong, X.Q., Chen, T., Roy, K., Held, G., Tsang, S.C.E., 2020. Methanol synthesis at a wide range of H_2/CO_2 ratios over a Rh-in bimetallic catalyst. Angew. Chem. Int. Ed. 59, 16039–16046. https://doi.org/10.1002/ANIE.202000841.

Lopez, G., Erkiaga, A., Amutio, M., Bilbao, J., Olazar, M., 2015. Effect of polyethylene co-feeding in the steam gasification of biomass in a conical spouted bed reactor. Fuel 153, 393–401. https://doi.org/10.1016/J.FUEL.2015.03.006.

Ma, Z., Porosoff, M.D., 2019. Development of tandem catalysts for CO_2 hydrogenation to olefins. ACS Catal. 9, 2639–2656. https://doi.org/10.1021/ACSCATAL.8B05060.

Marcos, F.C.F., Cavalcanti, F.M., Petrolini, D.D., Lin, L., Betancourt, L.E., Senanayake, S. D., Rodriguez, J.A., Assaf, J.M., Giudici, R., Assaf, E.M., 2022. Effect of operating parameters on H_2/CO_2 conversion to methanol over Cu-Zn oxide supported on ZrO_2 polymorph catalysts: characterization and kinetics. Chem. Eng. J. 427, 130947. https://doi.org/10.1016/J.CEJ.2021.130947.

Martin, O., Martín, A.J., Mondelli, C., Mitchell, S., Segawa, T.F., Hauert, R., Drouilly, C., Curulla-Ferré, D., Pérez-Ramírez, J., 2016. Indium oxide as a superior catalyst for methanol synthesis by CO_2 hydrogenation. Angew. Chem. 128, 6369–6373. https://doi.org/10.1002/ange.201600943.

Nieskens, D.L.S., Lunn, J.D., Malek, A., 2018. Understanding the enhanced lifetime of SAPO-34 in a direct syngas-to-hydrocarbons process. ACS Catal. 9, 691–700. https://doi.org/10.1021/acscatal.8b03465.

Palos, R., Gutiérrez, A., Vela, F.J., Olazar, M., Arandes, J.M., Bilbao, J., 2021. Waste refinery: the valorization of waste plastics and end-of-life tires in refinery units. A Review. Energy and Fuels 35, 3529–3557. https://doi.org/10.1021/acs.energyfuels.0c03918.

Pérez-Uriarte, P., Ateka, A., Aguayo, A.T., Gayubo, A.G., Bilbao, J., 2016. Kinetic model for the reaction of DME to olefins over a HZSM-5 zeolite catalyst. Chem. Eng. J. 302, 801–810. https://doi.org/10.1016/J.CEJ.2016.05.096.

Portillo, A., Ateka, A., Ereña, J., Aguayo, A.T., Bilbao, J., 2021. Conditions for the joint conversion of CO_2 and syngas in the direct synthesis of light olefins using In_2O_3–ZrO_2/SAPO-34 catalyst. Ind. Eng. Chem. Res. https://doi.org/10.1021/ACS.IECR.1C03556.

Pustovarenko, A., Dikhtiarenko, A., Bavykina, A., Gevers, L., Ramírez, A., Russkikh, A., Telalovic, S., Aguilar, A., Hazemann, J.L., Ould-Chikh, S., Gascon, J., 2020. Metal-organic framework-derived synthesis of cobalt indium catalysts for the hydrogenation of CO_2 to methanol. ACS Catal. 10, 5064–5076. https://doi.org/10.1021/ACSCATAL.0C00449.

Ramirez, A., Chowdhury, A.D., Dokania, A., Cnudde, P., Caglayan, M., Yarulina, I., Abou-Hamad, E., Gevers, L., Ould-Chikh, S., De Wispelaere, K., Van Speybroeck, V., Gascon, J., 2019. Effect of zeolite topology and reactor configuration on the direct conversion of CO_2 to light olefins and aromatics. ACS Catal. 9, 6320–6334. https://doi.org/10.1021/acscatal.9b01466.

Rui, N., Zhang, F., Sun, K., Liu, Z., Xu, W., Stavitski, E., Senanayake, S.D., Rodriguez, J. A., Liu, C.J., 2020. Hydrogenation of CO_2 to methanol on a $au^{\delta+}$-in_2O_{3-x}Catalyst. ACS Catal. 10, 11307–11317. https://doi.org/10.1021/ACSCATAL.0C02120.

Sánchez-Contador, M., Ateka, A., Aguayo, A.T., Bilbao, J., 2018. Behavior of SAPO-11 as acid function in the direct synthesis of dimethyl ether from syngas and CO_2. J. Ind. Eng. Chem. 63, 245–254. https://doi.org/10.1016/J.JIEC.2018.02.022.

Sehested, J., 2019. Industrial and scientific directions of methanol catalyst development. J. Catal. https://doi.org/10.1016/j.jcat.2019.02.002.

Snider, J.L., Streibel, V., Hubert, M.A., Choksi, T.S., Valle, E., Upham, D.C., Schumann, J., Duyar, M.S., Gallo, A., Abild-Pedersen, F., Jaramillo, T.F., 2019. Revealing the synergy between oxide and alloy phases on the performance of bimetallic in-Pd catalysts for CO_2 hydrogenation to methanol. ACS Catal. 9, 3399–3412. https://doi.org/10.1021/acscatal.8b04848.

Solis-Garcia, A., Louvier-Hernandez, J.F., Almendarez-Camarillo, A., Fierro-Gonzalez, J. C., 2017. Participation of surface bicarbonate, formate and methoxy species in the carbon dioxide methanation catalyzed by ZrO_2-supported Ni. Appl. Catal. B Environ. 218, 611–620. https://doi.org/10.1016/J.APCATB.2017.06.063.

Su, J., Wang, D., Wang, Y., Zhou, H., Liu, C., Liu, S., Wang, C., Yang, W., Xie, Z., He, M., 2018. Direct conversion of syngas into light olefins over zirconium-doped indium (III) oxide and SAPO-34 bifunctional catalysts: design of oxide component and construction of reaction network. ChemCatChem 10, 1536–1541. https://doi.org/10.1002/cctc.201702054.

Sun, K., Fan, Z., Ye, J., Yan, J., Ge, Q., Li, Y., He, W., Yang, W., Liu, C., 2015. Hydrogenation of CO_2 to methanol over In_2O_3 catalyst. J. CO2 Util. 12, 1–6. https://doi.org/10.1016/j.jcou.2015.09.002.

Tan, L., Zhang, P., Cui, Y., Suzuki, Y., Li, H., Guo, L., Yang, G., Tsubaki, N., 2019. Direct CO_2 hydrogenation to light olefins by suppressing CO by-product formation. Fuel Process. Technol. 196, 106174. https://doi.org/10.1016/j.fuproc.2019.106174.

Tian, P., Wei, Y., Ye, M., Liu, Z., 2015. Methanol to olefins (MTO): from fundamentals to commercialization. ACS Catal. 5, 1922–1938. https://doi.org/10.1021/acscatal.5b00007.

Wang, J., Zhang, G., Zhu, J., Zhang, X., Ding, F., Zhang, A., Guo, X., Song, C., 2021. CO_2 hydrogenation to methanol over In_2O_3-based catalysts: from mechanism to catalyst development. ACS Catal. 11, 1406–1423. https://doi.org/10.1021/acscatal.0c03665.

Wei, J., Ge, Q., Yao, R., Wen, Z., Fang, C., Guo, L., Xu, H., Sun, J., 2017. Directly converting CO_2 into a gasoline fuel. Nat. Commun. 81 8, 1–9. https://doi.org/10.1038/ncomms15174, 2017.

Wei, J., Yao, R., Han, Y., Ge, Q., Sun, J., 2021. Towards the development of the emerging process of CO_2 heterogenous hydrogenation into high-value unsaturated heavy hydrocarbons. Chem. Soc. Rev. 50, 10764–10805. https://doi.org/10.1039/D1CS00260K.

Ye, J., Liu, C., Ge, Q., 2012. DFT study of CO_2 adsorption and hydrogenation on the In_2O_3 surface. J. Phys. Chem. C 116, 7817–7825. https://doi.org/10.1021/jp3004773.

Ye, J., Liu, C., Mei, D., Ge, Q., 2013. Active oxygen vacancy site for methanol synthesis from CO_2 hydrogenation on In_2O_3 (110): a DFT study. ACS Catal. 3, 1296–1306. https://doi.org/10.1021/cs400132a.

Ye, J., Liu, C.J., Mei, D., Ge, Q., 2014. Methanol synthesis from CO_2 hydrogenation over a Pd_4/In_2O_3 model catalyst: a combined DFT and kinetic study. J. Catal. 317, 44–53. https://doi.org/10.1016/j.jcat.2014.06.002.

Ye, R.P., Ding, J., Gong, W., Argyle, M.D., Zhong, Q., Wang, Y., Russell, C.K., Xu, Z., Russell, A.G., Li, Q., Fan, M., Yao, Y.G., 2019. CO_2 hydrogenation to high-value products via heterogeneous catalysis. Nat. Commun. 10 https://doi.org/10.1038/S41467-019-13638-9.

Zhang, J., Lu, B., Chen, F., Li, H., Ye, M., Wang, W., 2018. Simulation of a large methanol-to-olefins fluidized bed reactor with consideration of coke distribution. Chem. Eng. Sci. 189, 212–220. https://doi.org/10.1016/J.CES.2018.05.056.

Zhang, Z., Pan, S.Y., Li, H., Cai, J., Olabi, A.G., Anthony, E.J., Manovic, V., 2020. Recent advances in carbon dioxide utilization. Renew. Sustain. Energy Rev. 125, 109799. https://doi.org/10.1016/J.RSER.2020.109799.